Effect of Thiophene Sequence Separation on Air-stable OTFT Materials

Shusuke Kanazawa, Musubu Ichikawa*, Youki Fujita, Ryu Koike,
Toshiki Koyama, and Yoshio Taniguchi

Faculty of Textile Science and Technology, Department of Functional Polymer Science,
Shinshu University, Ueda, Nagano 386-8567, JAPAN

* Corresponding author. Tel.: +81-268-21-5417; fax: +81-268-21-5413
E-mail address: musubu@shinshu-u.ac.jp (M. Ichikawa)

Abstract

The relationship between thiophene sequences and organic thin-film transistor (OTFT) characteristics was studied to determine their effect on ionization potential, molecular orientation, and air stability. Two types of molecular structures were used: continuous sequence and divided sequence thiophenes. The length of thiophene sequence did not affect FET characteristics but did affect ionic potential and air stability. Furthermore, materials with divided thiophene sequences showed no change in OTFT characteristics when exposed to air. These results suggest that separation of thiophene sequences can improve air stability, which is a problem of thiophene-based materials.

PACS: 73.61.Ph

Keywords: thiophene derivatives; organic transistors; ionization potential; air stability; thiophene sequence.

Introduction

Organic thin film transistors (OTFTs) have been the subject of a lot of recent research because they can be used in active matrix switching devices in flat panel displays due to their low cost, large area process ability, and flexibility [1−5]. Various organic semiconducting materials have been used in the active layers of OTFTs. Of these, thiophene-based derivatives are among the most attractive materials because their molecular structures can be easily modified using various organic synthesis methodologies such as introduction of substituents. For example, regio-regular poly(3-hexylthiophene) is a representative thiophene-based material that has performed

well in polymer TFTs [6] and organic solar cells [7]. Thiophene oligomers, which consist of several thiophene rings, have been reported to have charge carrier mobilities comparable to that of amorphous silicon [8−11]. Research has also been done on improving their electrical characteristics using crystal growth [12,13] including by self-assembly from solution [14]. Thiophene oligomers are also known as good photonic materials due to their excellent π-conjugation [15,16]. However, over time, atmospheric moieties such as oxygen tend to degrade the performance of most of these materials. This undesirable feature is due their low ionization potential (I_p), which causes high electron donation. It has been reported that longer thiophene sequences tend to reduce the I_ps of thiophene materials [17,18]. However, longer thiophene sequences can improve charge transport ability because their molecular interactions are strong [19,20]. Therefore, keeping a high I_p in materials with several thiophenes in a molecule is an important issue that must be addressed by designing thiophene-based materials that combine high mobility and good stability. To make the design of such a material possible, we studied the relationship between molecular structure and carrier transport characteristics. We investigated the four-thiophene molecules shown in Fig. 1 and demonstrated that split-sequence thiophenes have both large I_ps and good charge transport ability. A split-sequenced oligothiophene with single phenylene has been reported by Ponomarenko *et al* [17], here we demonstrate the effect on I_p again using biphenyl-splitting oligothiophene and clearly show the TFT stability in the air and briefly discuss the difference between one-phenyl and two-phenyls.

We studied the four four-thiophene materials shown in Fig. 1. Quaterthiophene (4T), which simply consists of four thiophenes, is a common p-type organic semiconductor. P4T and 4TC2P have two more phenylene rings than 4T. As can be seen in Fig. 1, P4T and 4TC2P are isomers of each other. In 4TC2Pme is identical to 4TC2P except that the α-positions of both of its end-thiophenes are methyl. These materials all have four thiophenes.

Results and Discussion

Ionization Potentials and Band Gaps of the Materials

Fig. 2 shows the photoelectron emission yield spectra of films of the materials. Their I_p values, which were estimated based on these spectra, are listed in Table 1. 4T and P4T showed similar I_ps in the lower energy range of about 5.2 eV, and 4TC2P and 4TC2Pme showed similar values in the higher energy range of about 5.5 eV. We think

this difference arises from the lengths of the thiophene sequences, not from the total number of thiophenes in the molecules. That is, the biphenyl-splitting makes I_p 0.3 eV higher than fully linked compounds. One the other hand, it was 0.1 eV higher in the case of the single-phenyl splitting [17]. So it can be mentioned that biphenyl-splitting can work more efficiently for increasing I_p. The band gaps of the materials, estimated based on the edges of longer UV-vis spectra wavelengths (not shown), are also listed in Table 1. Band gaps fell into the same two groups; materials with separated thiophene chains (4TC2P and 4TC2Pme) had larger gaps because of their limited π-conjugation development. This indicates that the linkage conditions of thiophene chains are important factors in the materials. 4TC2P and 4TC2Pme, which had high I_ps values, can be expected to be air-stable OTFT materials.

Molecular Orientation in the Thin-film State

Fig. 3 shows the results of X-ray diffraction (XRD) measurements of the materials. As can be seen in Fig. 3a, the pattern for 4T peaked at $2\theta = 6.00°$ (d =14.7 Å), i.e., the perpendicular orientation of the molecule. Other peaks, which appeared at $2\theta =$ 11.8°, $2\theta =$ 17.6°, $2\theta =$ 23.4°, correspond to higher order diffraction of d =14.7 Å. This is the same as a molecular orientation that has been reported for 4T film [21]. As can be seen in Fig. 3b−d, the other three materials showed similar tendencies. The molecular orientation of 4TC2P can be demonstrated using the unit cell shown in Fig. 4. According to the cell parameters, the XRD pattern of 4TC2P (Fig. 3c), it can be understood that peaks at $2\theta = 7.00°$ (d =12.7 Å), 10.5° (d =8.45 Å), 14.0° (d =6.32 Å), 17.5° (d =5.06 Å) and 21.1° (d =4.21 Å) correspond, respectively, to lengths of c/2, c/3, c/4, c/5, and c/6. These progressive peaks indicate that, like 4T molecules, 4TC2P molecules align perpendicularly in the film. However, it is thought that the peak at $2\theta =$ 19.4° (d =4.58 Å) arises from polymorphism because it does not match any of the axes of the 4TC2P unit cell. We think this polymorphism is based on lying orientation because peaks that correspond to the c axis of 4TC2P showed a shift in the 4TC2Pme spectrum due to the length of methyl. However, the polymorphism peak also appeared at the same degree in 4TC2P. This feature can also be found in the results for P4T, so it can be concluded that there may be both perpendicular and lying molecular orientations in the three materials other than 4T.

OTFT characteristics

Fig. 4 shows the characteristics of 4TC2P and 4TC2Pme OTFTs. Like 4T and P4T OTFTs, both devices showed p-type behavior. Table 2 shows the field effect

mobilities (μ_{FET}), threshold voltages (V_{th}), ON/OFF ratios, and subthreshold slopes of all the fabricated devices. The μ_{FET}s were calculated from the saturated drain current (I_D) with Equation (1), where C_i is the specific capacitance of the insulator, L is channel length, V_G is gate voltage, and W is channel width.

$$I_D = \mu_{FET} \frac{WC_i}{2L}(V_G - V_{th})^2 \qquad (1)$$

We first measured OTFT characteristics in vacuum conditions (about 2 x 10^{-2} Pa). While the ON/OFF ratios and the subthreshold slopes showed no major change for any of the devices, the V_{th}s showed two different tendencies. The materials with no substituents on their end-thiophenes (4T and 4TC2P) showed higher V_{th}s, and the substituted materials (P4T and 4TC2Pme) showed lower ones. Thus, it can be concluded that materials with substituents in the α-positions of their end-thiophenes are better OTFT materials because of their lower V_{th}. However, the μ_{FET}s of all four OTFTs are about the same. This indicates that the carrier transport properties of materials with the same number of thiophenes are about the same even if they fully link to each other or divide into two parts.

The next thing we measured was characteristics of the devices when they were exposed to air. The measurements were done immediately after exposing the devices to the atmosphere. The OTFT characteristics when the devices were exposed to air are shown in Table 2, where it can be seen that all of the devices worked as well as in the vacuum condition. However, the 4TC2P device had significant hysteresis, as shown in Fig. 6. In contrast, as in the vacuum condition, the 4TC2Pme OTFT had no hysteresis (Fig. 6 inset). This difference suggests that the lack of substituents on both end-thiophenes degrades performance of OTFT materials. This notion is supported by the V_{th} behavior of other devices: 4T showed hysteresis but P4T did not. In addition, the similar result is previously reported using other thiophene derivatives [22]. Therefore, the high reactivity of the α-position of both end-thiophenes must be important.

We also measured the OTFT characteristics of these devices continuously for ten days to investigate the stability of the devices when they were left in the atmosphere. Fig. 7 shows storage time dependences for (a) V_{th} and (b) μ_{FET} of the devices made of 4T, 4TC2P, and 4TC2Pme. As expected, the 4TC2P and 4TC2Pme devices showed no change in V_{th} during the measurements, while the V_{th} of the 4T device decreased. This air stability must be due to the higher I_p caused by the divided thiophene linkage. However, the 4TC2P and 4TC2Pme devices showed different μ_{FET} behaviors, i.e., the μ_{FET} of the 4TC2Pme device did not change but that of 4TC2P decreased to about 20% of its initial value. The structural difference between the two materials is in their

end-thiophenes. The μ_{FET} of 4T, incidentally, also decreased. Therefore, to make thiophene materials air-stable, it is important both to maintain a large I_p and to substitute active α-positions for the end-thiophenes. As mentioned above, we successfully demonstrated that molecular structures like 4TC2Pme, with separated thiophene chains and substituted end-thiophenes, are air-stable thiophene derivatives.

Conclusion

We investigated the relationship between air-stability and molecular structure in materials that contain four thiophenes and whose molecular orientations in the thin-film state were about the same. I_ps were classified by type of thiophene chain, i.e., fully linked or divided. OTFTs made of these materials showed two tendencies with regard to air-stability. First, OTFTs made of materials with no substituents on the end-thiophenes, showed hysteresis in I_D-V_G characteristics. Second, materials with fully linked thiophenes showed changes in switching performance over time. This means that 4TC2Pme, which has two separate thiophene chains and substituents at both ends of the molecule, has both the normal advantages of thiophenes and significant stability as carrier transport material exposed to air.

Experimental

Synthesis

All reactions were carried out in an Ar environment. Solvents were purified according to the standard methods before use. A ^{1}H NMR (400 MHz) spectrum was recorded on a Bruker AVANCE-400 spectrometer, and chemical shifts (δ) were given in ppm relative to tetramethylsilane (TMS) as an internal standard. High-resolution mass (HRMS) measurements were carried out on a Jeol MS-700 spectrometer. The 4T was purchased from Sigma-Aldrich, and the P4T was prepared as recommended in the literature [23].

Preparation of 4TC2P

To a solution of 4,4’-diiodobiphenyl (1.0 g, 2.5 mmol) and 5-(4,4,5,5-tetramethyl-1,3,2-dioxaborolan-2-yl)-2,2'-bithiophene (1.8 g, 6.2 mmol) in toluene (40 mL) was added a 10% aqueous K_2CO_3 (30 ml). The contents were bubbled with nitrogen for 30 min to remove soluble oxygen, then tetrakis(triphenylphosphine)

palladium(0) (0.028 g, 0.024 mmol, $Pd(Ph_3)_4$) was added and the solution refluxed for 18 h. After the solution was cooled to room temperature, the precipitate was filtrated and sequentially washed with toluene, distilled water, and methanol to produce crude 4TC2P, which was purified by the sublimation method described below. HRMS (EI) calcd for $C_{28}H_{18}S_4$ $[M]^+$ 482.0291 found 482.0316.

Preparation of 4TC2Pme

4TC2Pme was prepared from 5-(4,4,5,5-tetramethyl-1,3,2-dioxaborolan-2-yl)-5'-methy-l-2,2'-bithiophene (100 mg, 0.33 mmol, this compound was synthesized as described in the next section "Preparation of 5-(4,4,5,5-tetramethyl-1,3,2-dioxaborolan-2-yl)-5'-methyl-2,2'-bithiophene"), 4,4'-diiodobiphenyl (66.3 mg, 0.16 mmol), and $Pd(PPh_3)_4$ (11.3 mg, 0.0098 mmol) in a manner similar to a to that described above. HRMS (EI) calcd for $C_{30}H_{22}S_4$ $[M]^+$ 510.0604, found 510.0609.

Preparation of 5-(4,4,5,5-tetramethyl-1,3,2-dioxaborolan-2-yl)-5'-methyl-2,2'-bithiophene

To a solution of 5-methyl-2,2'-bithiophene (420 mg, 2.3 mmol) and *N,N,N',N'*-tetramethylenediamine (0.38 mL, 2.56 mmol) in THF (50 mL) was added dropwise a 1.6 mol/L *n*-BuLi in hexane (1.6 mL, 2.56 mmol) at -78ºC. After being stirred for 15 min, 2-isopropoxy-4,4,5,5-tetramethyl-1,3,2-dioxaborolane (0.48 g, 2.56 mmol) was added and stirred for 1 h, then reacted for 24 h at room temperature.

Saturated aqueous NH_4Cl (3 drops) was added to a reaction mixture to quench an excess *n*-BuLi and extracted with ethyl acetate. The organic phase was washed with brine and then dried over anhydrous $MgSO_4$. The solvent was removed under the reduced pressure. The residue was purified by the silica gel column-chromatography (eluent: hexane) to give 5-(4,4,5,5-tetramethyl-1,3,2-dioxaborolan-2-yl)-5'-methyl-2,2'-bithiophene (60%). ^{1}H NMR ($CDCl_3$) δ : 1.35 (s, 12H, C*H*$_3$), 2.48 (s, 3H, C*H*$_3$), 6.64 (d, 1H, Ar-*H*, *J* = 3.6 Hz), 7.03 (d, 1H, Ar-*H*, *J* = 3.6 Hz), 7.15 (d, 1H, Ar-*H*), 7.50 (d, 1H, Ar-*H*).

The 4T, P4T, 4TC2P, and 4TC2Pme were used for other experiments after further purification by thermal gradient sublimation.

Fabrication and measurement

We fabricated top-contact OTFTs made of the organic materials (4T, P4T, 4TC2P, and 4TC2Pme). The OTFTs were prepared on heavily doped n-type silicon wafers with 400-nm-thick thermally grown SiO_2, which were used as a gate electrode

and a gate dielectric (specific capacitance of 7.5 nF/cm^2), respectively. The organic materials were thermally evaporated at the rate of 0.4 Å/s onto room temperature substrates. The pressure in the evaporation chamber was 4.0 x 10^{-6} Torr, and the organic layers were 60–nm thick. Finally, Au was thermally evaporated onto the organic layers through a shadow mask to form source and drain electrodes. The channel length and width were 30 μm and 2 mm, respectively. OTFT characteristics were measured in a vacuum (below 5 x 10^{-2} Pa) and in the atmosphere using two KEITHLEY 2410 source meters.

The photoelectron emission yield spectra were measured with a Riken-Keiki AC2 at an irradiation light power of 10 nW/cm^2. The sample films of the organic materials were prepared by vacuum evaporation in the same conditions as were used to fabricate OTFTs on glass substrates whose surface was covered with indium thin oxide. The organic films were 100–nm thick.

The X-ray diffraction patterns were measured with a Rigaku Rotaflex using Cu $K\alpha$ radiation at $\theta/2\theta$ geometry. The sample films, which all had thicknesses of 100 nm, were evaporated onto silicon wafers with SiO_2 in the same conditions as were used for TFT fabrication. The X-ray was generated from a 150-mA-electron beam accelerated at 40 kV. The crystal structure was analyzed with a Bruker AXS APEXⅡ from Bruker AXS Japan Co. Ltd.

Acknowledgements

This work was supported by the Cooperative Link for Unique Science and Technology for Economy Revitalization (CLUSTER) and CLUSTER (the second stage), programs of the Japanese Ministry of Education, Culture, Sports, Science and Technology. The authors thank Bruker AXS Japan Co. Ltd. for analyzing the crystal structure of the 4TC2P.

References

[1] G. Horowitz, D. Fichou, X. Peng, Z. Xu, F. Garnier, Solid State Commun. 72 (1989) 381.

[2] G. Horowitz, M. E. Hajlaoui, Adv. Mater. 12 (2000) 1046.

[3] C. D. Dimitrakopoulos, P. R. L. Malenfant, Adv. Mater. 14(2002) 99.

[4] C. D. Sheraw, L. Zhou, J. R. Huang, D. J. Gundlach, T. N. Jackson, M. G. Kane, I. G. Hill, M. S. Hammond, J. Campi, B. K. Greening, J, Francl, J. West, Appl. Phys Lett. 80 (2002) 1088.

[5] F. Eder, H. Klauk, M. Halik, U. Zschieschang, G. Schmid, C. Dehm, Appl. Phys. Lett. 84 (2004) 2673.

[6] H. Yang, T. J. Shin, L. Yang, K. Cho, C. Y. Ryu, Z. Bao, Adv. Funct. Mater. 15 (2005) 671.

[7] Y. Kim, S. Cook, S. M. Tuladhar, S. A. Choulis, J. Nelson, J. R. Durrant, D. D. C. Bradley, M. Giles, I. Mcculloch, C.-S. Ha, M.Ree, Nature Materials 5 (2006) 197.

[8] M. Ichikawa, H. Yanagi, Y. Shimizu, S. Hotta, N. Suganuma, T. Koyama, Y. Taniguchi, Adv. Mater. 14 (2002) 1272.

[9] K. Nakamura, M. Ichikawa, R. Fushiki, T. Kamikawa, M. Inoue, T. Koyama, Y. Taniguchi, Jpn. J. Appl. Phys. 43 (2004) L100-L102.

[10] B. Wex, B. R. Kaafarani, R. Schroeder, L. A. Majewski, P. Burckel, M. Grell, D. C. Neckers, J. Mater. Chem. 16 (2006) 1121-1124.

[11] Y. Sun, Y. Liu, Y. Ma, C. Di, Y. Wang, W. Wu, G. Yu, W. Hu, D. Zhu, Appl. Phys. Lett. 88 (2006) 242113.

[12] J. Ackermann, C. Videlot, P. Dumas, A. E. Kassmi, R. Guglielmetti, V. Safalov, Oraganic Electronics, 5 (2004) 213-222.

[13] S. Kanazawa, M. Ichikawa, T. Koyama, Y. Taniguchi, ChemPhysChem 7 (2006) 1881-1884.

[14] M. Funahashi, F. Chang, N. Tamaoki, Adv. Mater. 19 (2007) 353.

[15] M. Ichikawa, R. Hibino, M. Inoue, T. Haritani, S. Hotta, T. Koyama, Y. Taniguchi, Adv. Mater. 15 (2003) 213.

[16] C. V. Ackermann, T. Isoshima, A. Yassar, T. Wada, H. Sasabe, D. Fichou, Synth. Met. 156 (2006) 154-161.

[17] S. A. Ponomarenko, S. Kirchmeyer, M. Halik, H. Klauk, U. Zschieschang, G. Schmid, A. Karbach, D. Dreschsler, N. M. Alpatova, Synth. Met. 149 (2005) 231-235.

[18] A. J. Mäkinen, I. G. Hill, M. Kinoshita, T. Noda, Y. Shirota, Z. H. Kafari, J. Appl. Phys. 91 (2002) 5456.
[19] M. Halik, H. Klauk, U. Zschieschang, G. Schmid, S. Ponomarenko, S. Kirchmeyer, W. Weber, Adv. Mater. 15 (2003) 917.
[20] C. V. Ackermann, J. Ackermann, H. Brisset, K. Kawamura, N. Yoshimoto, P. Raynal, A. E. Kassmi, F. Fages, J. Am. Chem. Soc. 127 (2005) 16346.
[21] J. Vrijmoeth, R. W. Stok, R. Veldman, W. A. Schoonveld, T. M. Klapwijk, J. Appl. Phys. 83 (1998) 3816.
[22] C. V. Ackermann, J. Ackermann, K. Kawamura, N. Yoshimoto, H. Brisset, P. Raynal, A. E. Kassmi, F. Fages, Organic electronics 7 (2006) 465-473.
[23] S. Hotta, S. A. Lee, T. Tamaki, J. Heterocyclic Chem. 37 (2000) 25.

Table 1. Energies of I_p and band gap of materials.

	I_p (eV)	Band Gap (eV)
4T	5.24	2.53
P4T	5.20	2.53
4TC2P	5.52	2.62
4TC2Pme	5.53	2.62

Table 2. Characteristics of oligomer material OTFTs in vacuum. Characteristics in atmosphere are shown in parentheses.

	μ_{FET} (cm^2/Vs)	V_{th} (V)	ON/OFF ratio	subthreshold slope (V/decade)
4T	3.7×10^{-2} (3.1×10^{-2})	-30 (-33)	10^4 (10^4)	8 (7)
P4T	5.3×10^{-2} (5.4×10^{-2})	-25 (-30)	10^4 (10^4)	8 (10)
4TC2P	2.1×10^{-2} (2.6×10^{-2})	-36 (-40)	10^4 (10^4)	9 (7)
4TC2Pme	5.2×10^{-2} (4.7×10^{-2})	-21 (-20)	10^4 (10^4)	8 (8)

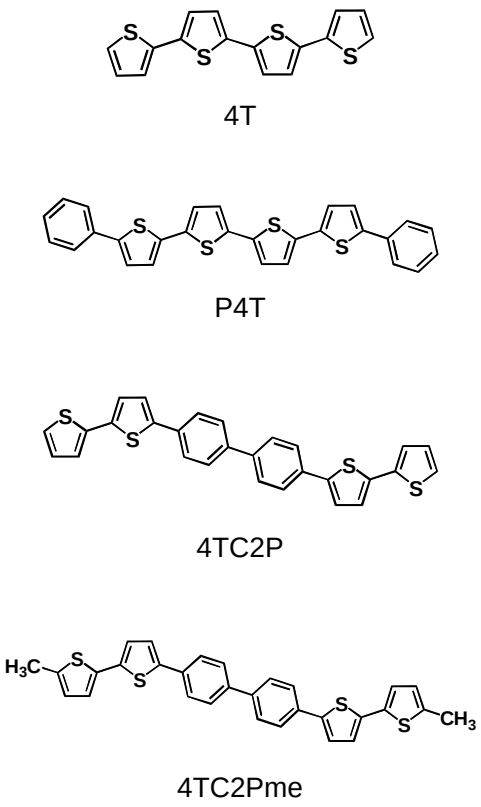

Fig. 1. Chemical structures of materials used.

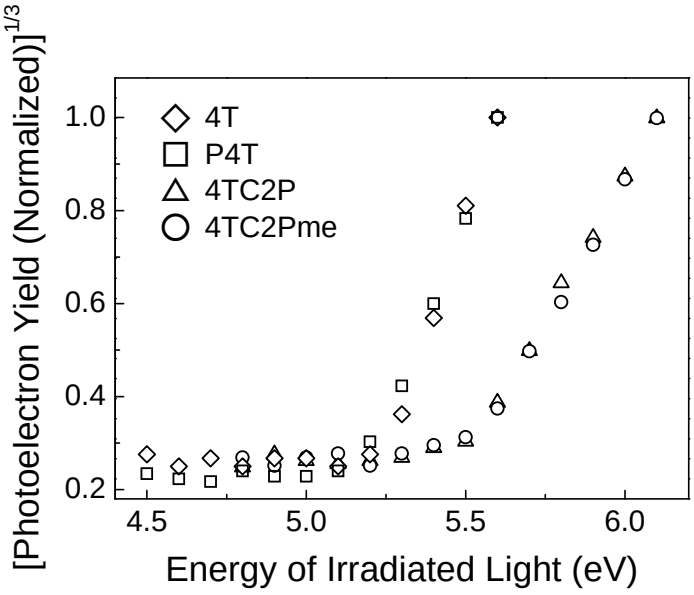

Fig. 2. Photoelectron emission yield spectra of materials.

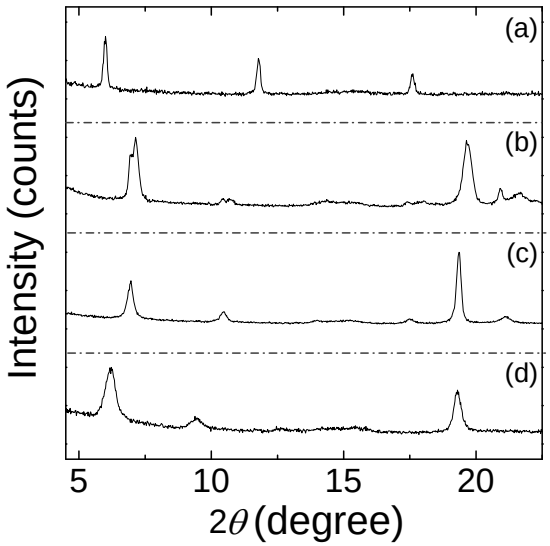

Fig. 3. XRD patterns of (a) 4T, (b) P4T, (c) 4TC2P, and (d) 4TC2Pme films.

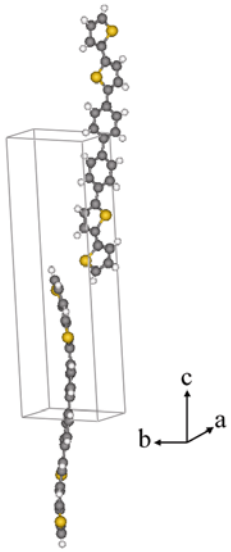

Fig. 4. 4TC2P unit cell. (Crystal class: monoclinic, Space group: *P21*, Cell Constants: a = 5.816 Å; b = 7.2527 Å; c = 25.2863 Å; β = 96.265°;
CCDC number: 673710, the crystallographic data can be obtained free of charge from the Cambridge Crystallographic Data Centre via www.ccdc.cam.ac.uk/data_request/cif.)

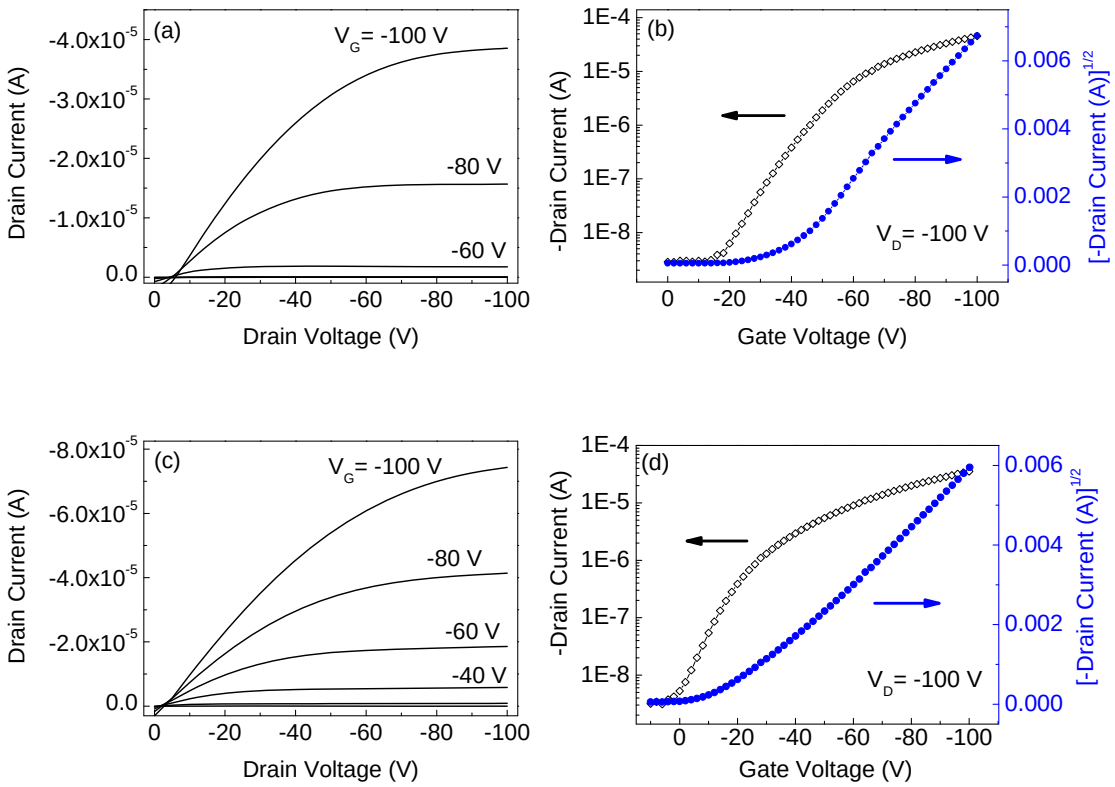

Fig. 5. I_D-V_D characteristics and I_D-V_G characteristics of (a, b) 4TC2P and (c, d) 4TC2Pme.

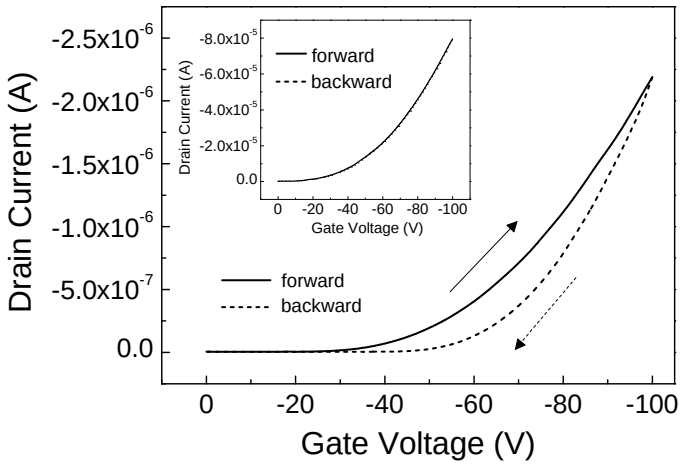

Fig. 6. Forward (solid line) and backward (dotted line) I_D-V_D characteristics of 4TC2P OTFTs and (inset) 4TC2Pme OTFTs.

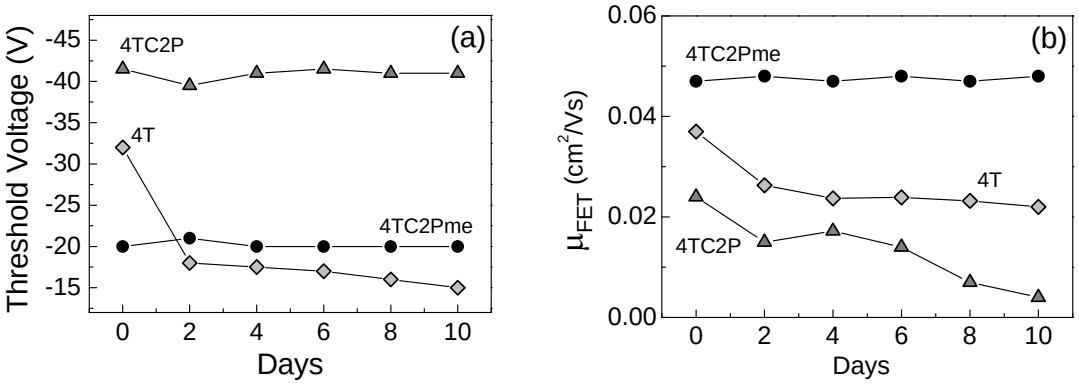

Fig. 7. Storage time dependences of (a) threshold voltage and (b) field-effect mobility of (◆) 4T, (▲) 4TC2P, and (●) 4TC2Pme OTFTs.

.